International Journal of Fracture **107:** 73–98, 2001.

Transient thermal stress analysis of an edge crack in a functionally graded material

Z.-H. JIN and GLAUCIO H. PAULINO*
Department of Civil and Environmental Engineering, University of Illinois at Urbana-Champaign, Urbana, IL 61801, USA
*(*Author for correspondence: fax: (217) 265-8041; e-mail: paulino@uiuc.edu)*

Received 24 January 2000; accepted in revised form 20 June 2000

Abstract. An edge crack in a strip of a functionally graded material (FGM) is studied under transient thermal loading conditions. The FGM is assumed having constant Young's modulus and Poisson's ratio, but the thermal properties of the material vary along the thickness direction of the strip. Thus the material is elastically homogeneous but thermally nonhomogeneous. This kind of FGMs include some ceramic/ceramic FGMs such as TiC/SiC, $MoSi_2/Al_2O_3$ and $MoSi_2$/SiC, and also some ceramic/metal FGMs such as zirconia/nickel and zirconia/steel. A multi-layered material model is used to solve the temperature field. By using the Laplace transform and an asymptotic analysis, an analytical first order temperature solution for short times is obtained. Thermal stress intensity factors (TSIFs) are calculated for a TiC/SiC FGM with various volume fraction profiles of the constituent materials. It is found that the TSIF could be reduced if the thermally shocked cracked edge of the FGM strip is pure TiC, whereas the TSIF is increased if the thermally shocked edge is pure SiC.

Key words: Fracture mechanics, stress intensity factor, functionally graded material, thermal stress, heat conduction.

1. Introduction

Ceramic materials represent one of the most promising materials for future technologies of aerospace, nuclear and other engineering applications because of their excellent properties at high temperatures and their superior corrosion and wear resistance. One major limitation of ceramics is their inherent brittleness that can result in catastrophic failure under severe thermal shock loads. To overcome this disadvantage, considerable efforts have been made to toughen ceramics with some success. On the other hand, for ceramics in high temperature applications, one may specifically design the material to reduce thermal stresses when subjected to a thermal shock. This is one of the objectives to be fulfilled by the concept of functionally graded materials (FGMs)(Koizumi, 1993; Hirai, 1996; Suresh and Mortensen, 1998). An FGM is a multi-phase material with the volume fractions of the constituents varying gradually in a pre-determined profile, thus giving a non-uniform micro-structure in the material with continuously graded macro-thermomechanical properties. By introducing thermal conductivity gradient, Hasselman and Youngblood (1978) showed that significant reductions in the magnitude of the tensile thermal stress in ceramic cylinders could be achieved. Thermal residual stresses may be relaxed in a metal-ceramic layered material by inserting a functionally graded interface layer between the metal and the ceramic (Kawasaki and Watanabe, 1987; Drake et al., 1993; Giannakopoulos et al., 1995). When subjected to thermal shocks, FGM

coatings may suffer significantly less damage than conventional ceramic coatings (Kuroda et al., 1993; Takahashi et al., 1993).

The knowledge of fracture behavior of FGMs is important in order to evaluate their integrity. The existing analytical studies in this aspect have been mainly related to crack growth behavior in FGMs with specific material properties. By assuming an exponential spatial variation of elastic modulus, Delale and Erdogan (1983), Erdogan (1995) and Erdogan and Wu (1997) solved crack problems under mechanical loading conditions. Gu and Asaro (1997a) calculated the stress intensity factor (SIF) for a semi-infinite crack in both isotropic and orthotropic materials. They also studied crack deflection problem in FGMs (Gu and Asaro, 1997b). Honein and Herrmann (1997) studied conservation laws for inhomogeneous elastic materials and obtained the SIF for a semi-infinite crack by using the path-independent integral that they proposed. Since the material properties in those studies were specifically assumed, the SIF concept could be well defined. For general inhomogeneous materials, Schovanec and Walton (1988) and Jin and Noda (1994a) showed that the crack tip fields are identical to those in homogeneous materials provided that the material properties are continuous and piecewise differentiable. Hence, the SIF can still be used to study fracture behavior of FGMs as long as the crack tip nonlinear deformations and process zones are completely included within the region dominated by the SIF. The SIF dominant (K-dominant) zone, however, may be reduced significantly if the modulus gradient is very large. Jin and Batra (1996a) gave a rough estimate on the effect of modulus gradients in the K-dominant zone. They also studied crack growth resistance curve (R-curve) in FGMs using both rule of mixtures and crack-bridging concepts. The effect of loading conditions and specimen size on the R-curve and residual strength behavior were also investigated (Jin and Batra, 1996a; 1998). Cai and Bao (1998) performed a crack-bridging analysis to predict crack propagation in FGM coatings. Using a finite element method, Bao and Wang (1995) studied multi-cracking in an FGM coating. Carpenter et al. (1999) presented a testing protocal and analysis for a sub-scale FGM specimen suitable for experimental measurement of critical SIF and $J-R$ curve. Paulino et al. (1999) analyzed an antiplane shear crack in an FGM in the context of gradient elasticity.

For thermal loading problems, by assuming exponential variations in both elastic and thermal properties, Noda and Jin (1993) and Erdogan and Wu (1996) computed steady thermal stress intensity factors (TSIFs) for cracks in thermally loaded FGM strips. Jin and Noda (1994b) and Jin and Batra (1996b) also considered cracks subjected to transient thermal loads. Choi et al. (1998) studied cracking in a layered material with an FGM interfacial zone subjected to a thermal shock. Using both experimental and numerical techniques, Kokini and Choules (1995) and Kokini and Case (1997) investigated surface and interface cracking in FGM coatings subjected to thermal shocks. By employing a finite element method, Noda (1997) analyzed an edge crack problem in a zirconia/titanium FGM plate subjected to cyclic thermal loads. Reddy and Chin (1998) performed a thermomechanical analysis of FGM cylinders and plates under bending. Aboudi et al. (1997) examined microstructural optimization of FGMs subjected to a thermal gradient via the coupled higher order theory. Joachim-Ajao and Barber (1998) have studied the effect of material properties in thermoelastic contact problems. Georgiadis et al. (1991) presented an asymptotic solution for short-time transient heat conduction between two dissimilar bodies in contact. All the above references focus on FGMs, except the last two, which have a more general scope.

In this paper, an edge crack in an FGM strip under transient thermal loading conditions is studied (see Figure 1). The FGM is assumed having constant Young's modulus and Poisson's ratio, but the thermal properties of the material vary along the thickness direction of the strip.

A multi-layered material model is used to solve the temperature field. By using Laplace transform and asymptotic analysis, an analytical first order temperature solution for short times is obtained. Thermal stresses and TSIFs are calculated for a TiC/SiC FGM, and the effect of the volume fraction profiles of the constituent materials on thermal stresses and TSIFs is discussed.

General purpose numerical methods such as the finite element method (FEM) or the boundary element method (BEM) can be used to tackle the problem investigated here. However, the standard FEM leads to undesirable jumps in derivative response quantities (e.g., fluxes and stresses) at bimaterial interfaces. Moreover, these methods require a discretization process which is time consuming and may require several iteration steps for achieving the desired accuracy level. The present contribution combines analytical techniques with the integral equation method to solve heat transfer and edge crack problems in FGM strips subjected to transient thermal loading conditions by means of a multi-layered material model with arbitrary number of layers. Thus the solution for this class of problems can be obtained effectively, efficiently and accurately.

2. Temperature field

A thermal conduction problem for an FGM strip is described, a multi-layered material model is introduced, and its discretization is discussed. The classical temperature solution for a homogeneous material is presented and limitations of applying the solution to the layered material model is pointed out. The solution approach taken here aims at overcoming the complexity of existing temperature solutions based on multi-layered material model in the literature. Thus, a feasible solution approach is given here by means of the Laplace transform technique. To avoid difficulties associated with the numerical inversion of the Laplace transform, a closed form analytical solution is sought. This is fulfilled by inverting the Laplace transform of the temperature for large values of their argument. Thus an analytical asymptotic solution of temperature for short times is obtained. This asymptotic solution is the main contribution of the present work in the sense that it allows to study the effect of volume fraction profiles in FGMs on the thermal stress and thermal fracture (see Section 6).

2.1. Multi-layered material model

Consider an infinite strip of thickness b with an edge crack of length a as shown in Figure 1. The strip is initially at a constant temperature. Without loss of generality, the initial constant temperature can be assumed as zero. The surfaces $X = 0$ and $X = b$ of the strip are suddenly cooled down to temperatures $-T_0$ and $-T_b$, respectively. Since the heat will flow only in the X-direction, the initial and boundary conditions for the temperature field are

$$T = 0, \qquad t = 0, \tag{1}$$

$$T = -T_0, \quad X = 0, \tag{2}$$

$$T = -T_b, \quad X = b. \tag{3}$$

Here an idealized thermal shock boundary condition is assumed, i.e., the heat transfer coefficient on the surfaces of the FGM strip is infinitely large. This corresponds the most severe thermal stress induced in the strip. In other words, the thermal stress will be lower if a finite heat transfer coefficient is used. Later, we will discuss the effect of a finite heat transfer coefficient on the solution method developed in this section.

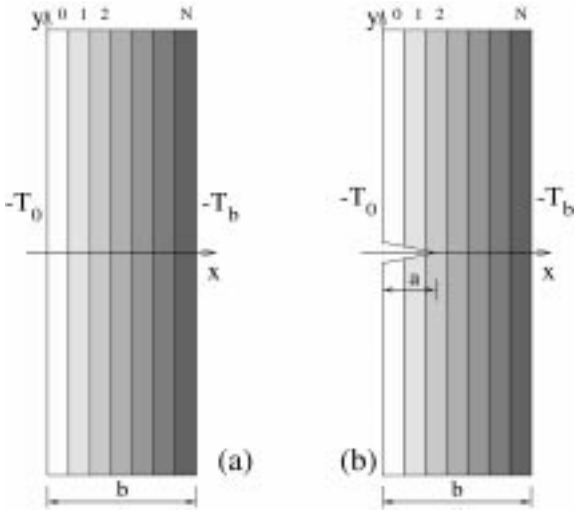

Figure 1. An FGM strip occupying the region $0 \leq x \leq b$ and $|y| < \infty$. The bounding surfaces of the strip are subjected to uniform thermal loads T_0 and T_b. (a) a layered material; (b) an edge crack in the layered material.

The heat flow is controlled by the following conduction equation

$$\frac{\partial}{\partial X}\left[k(X)\frac{\partial T}{\partial X}\right] = \rho(X)c(X)\frac{\partial T}{\partial t}. \tag{4}$$

where T is the temperature field, t the time, $k(X)$ the thermal conductivity, $\rho(X)$ the mass density and $c(X)$ the specific heat. Tanigawa et al. (1996) used a laminated material model to solve (4). They modeled the FGM by a laminated composite and each lamina was assumed as a homogeneous layer. With this model, they were able to obtain the temperature field in a similar way to that described by Ozisik (1980) for the heat conduction in a laminated composite material. The disadvantage of their analysis method is that to ensure convergence of the series solution, one has to numerically determine a sufficiently large number of the roots (eigenvalues) of a transcendental equation and the transcendental function is a determinant whose order is twice the number of layers which may become very large if the FGM strip is to be reasonably modeled by a layered material. This is particularly true for small times at which the solution series converges very slowly. *In this study, we also use a discrete model, i.e., the FGM strip is devided into many layers in the X-direction, say $N+1$ layers, as shown in Figure 1, and in each layer, the material properties are assumed as constants. However, we first determine the temperatures at the interfaces between layers and represent intra-layer temperatures by those interface temperatures without solving an eigenvalue problem. Further, an asymptotic temperature solution for small times is obtained here.*

The heat conduction equation in the nth homogeneous layer is given by

$$\frac{\partial^2 T}{\partial X^2} = \frac{1}{\kappa_n}\frac{\partial T}{\partial t}, \quad X_n < X < X_{n+1}, \quad n = 0, 1, ..., N, \tag{5}$$

where X_n and X_{n+1} are the $X-$ coordinates of the two boundaries of the nth layer and κ_n is the thermal diffusivity of the layer given by[1]

$$\kappa_n = k_n/(\rho_n c_n), \quad n = 0, 1, ..., N, \tag{6}$$

in which k_n, ρ_n and c_n are the thermal conductivity, mass density and specific heat of the nth layer. Here it is understood that $X_0 = 0$ and $X_{N+1} = b$. The temperatures at the boundaries of the nth layer are assumed as $T_n(t)$ and $T_{n+1}(t)$, respectively. Hence, the conditions for the nth layer are

$$\begin{aligned} T &= 0, && t = 0, \\ T &= T_n(t), && X = X_n, \\ T &= T_{n+1}(t), && X = X_{n+1}. \end{aligned} \tag{7}$$

Note that $T_0(t) = -T_0$ and $T_{N+1}(t) = -T_b$. By assuming the above conditions, the following temperature continuity conditions (Carslaw and Jaeger, 1959) at the interfaces between the layers are satisfied

$$T|_{X\to X_n^+} = T|_{X\to X_n^-}, \quad n = 1, 2, ..., N. \tag{8}$$

The N unkown interface temperatures, $T_n(t)$, ($n = 1, 2, ..., N$), are to be determined by the heat flux continuity conditions (Carslaw and Jager, 1959) at the interfaces between the layers

$$k_{n-1}\frac{\partial T}{\partial X}\Big|_{X\to X_n^-} = k_n \frac{\partial T}{\partial X}\Big|_{X\to X_n^+}, \quad n = 1, 2, ..., N. \tag{9}$$

The continuity conditions (8) and (9) were employed by Gray and Paulino (1997) to solve general interface and multi-zone problems for finite geometries by means of the symmetric Galerkin boundary element method.

2.2. Temperature solution in terms of interface temperatures

The temperature solution in the nth layer under the conditions (7) is well known and can be found in heat conduction books, for example, Carslaw and Jaeger (1959), as follows

$$\begin{aligned} T(x,t) = {} & \frac{2\kappa_n}{h_n}\sum_{\ell=1}^{\infty}\frac{\ell\pi}{h_n}\exp(-\kappa_n\ell^2\pi^2 t/h_n^2)\sin\left(\frac{\ell\pi x}{h_n}\right)\times \\ & \times\int_0^t \exp(\kappa_n\ell^2\pi^2 t'/h_n^2)\left[T_n(t') - (-1)^{\ell}\, T_{n+1}(t')\right]\mathrm{d}t', \\ & 0 < x < h_n, \quad n = 0, 1, ..., N, \end{aligned} \tag{10}$$

where x is the local coordinate and h_n is the thickness of the nth layer given by

$$x = X - X_n, \quad h_n = X_{n+1} - X_n, \tag{11}$$

respectively. The above expression of the temperature field can not be used in (9) to determine the unknowns $T_n(t)$ as the right hand side series does not converge uniformly in the interval

[1]The symbols k and κ should not be confused. Note that k denotes thermal conductivity and κ denotes thermal diffusivity.

considered. Thus the following alternative form for the temperature is used (Ozisik, 1980)

$$
\begin{aligned}
T(x^*,\tau) = (1-x^*)T_n(\tau) + x^* T_{n+1}(\tau) - \\
-2\sum_{\ell=1}^{\infty} \frac{\sin(\ell\pi x^*)}{\ell\pi}\left[T_n(\tau) - \beta_{\ell n}\int_0^{\tau} \exp(-\beta_{\ell n}(\tau-\tau'))T_n(\tau')\,\mathrm{d}\tau'\right] + \\
+2\sum_{\ell=1}^{\infty}(-1)^{\ell}\frac{\sin(\ell\pi x^*)}{\ell\pi}\left[T_{n+1}(\tau) - \beta_{\ell n}\int_0^{\tau} \exp(-\beta_{\ell n}(\tau-\tau'))T_{n+1}(\tau')\,\mathrm{d}\tau'\right], \\
0 < x^* < 1, \quad n = 0, 1, ..., N, \qquad (12)
\end{aligned}
$$

where x^* and τ are nondimensional space coordinate and time

$$x^* = x/h_n = (X - X_n)/(X_{n+1} - X_n), \qquad (13)$$

$$\tau = t\kappa_0/b^2, \qquad (14)$$

respectively, and $\beta_{\ell n}$ is a constant defined by

$$\beta_{\ell n} = \frac{\kappa_n}{\kappa_0}\left(\frac{b}{h_n}\right)^2 (\ell\pi)^2. \qquad (15)$$

The unknown interface temperatures $T_n(\tau)$ may be determined by substituting the temperature solution (12) into the interface conditions (9). This will result in a system of Volterra integral equations of $T_n(\tau)$ as follows

$$
\begin{aligned}
&\frac{k_{n-1}}{k_n}\{T_n(\tau) - T_{n-1}(\tau) - \\
&-2\sum_{\ell=1}^{\infty}(-1)^{\ell}[(T_{n-1}(\tau) - \beta_{\ell(n-1)}\int_0^{\tau} \exp(-\beta_{\ell(n-1)}(\tau-\tau'))T_{n-1}(\tau')\,\mathrm{d}\tau'] + \\
&+2\sum_{\ell=1}^{\infty}[(T_n(\tau) - \beta_{\ell(n-1)}\int_0^{\tau} \exp(-\beta_{\ell(n-1)}(\tau-\tau'))T_n(\tau')\,\mathrm{d}\tau']\} \\
&= \frac{h_{n-1}}{h_n}\{T_{n+1}(\tau) - T_n(\tau) - \\
&-2\sum_{\ell=1}^{\infty}[T_n(\tau) - \beta_{\ell n}\int_0^{\tau} \exp(-\beta_{\ell n}(\tau-\tau'))T_n(\tau')\,\mathrm{d}\tau'] + \\
&+2\sum_{\ell=1}^{\infty}(-1)^{\ell}[(T_{n+1}(\tau) - \beta_{\ell n}\int_0^{\tau} \exp(-\beta_{\ell n}(\tau-\tau'))T_{n+1}(\tau')\,\mathrm{d}\tau']\}, \\
&n = 1, 2, ..., N. \qquad (16)
\end{aligned}
$$

It is evident that the above equation is not appropriate to numerically determine the unknowns $T_n(\tau)$ because the series involved converge slowly and, more importantly, the convergence is dependent on the yet to be determined $T_n(\tau)$. To overcome this difficulty, we do not determine $T_n(\tau)$ by direct use of (16). Instead, we will study the problem in the Laplace transformed

plane and try to first obtain the Laplace transforms of $T_n(\tau)$. By applying Laplace transform to (16) and using the convolution theorem, we have

$$\frac{k_{n-1}}{k_n}\left\{\bar{T}_n(s)\left[1+2\sum_{\ell=1}^{\infty}\frac{s}{s+\beta_{\ell(n-1)}}\right]-\bar{T}_{n-1}(s)\left[1+2\sum_{\ell=1}^{\infty}(-1)^{\ell}\frac{s}{s+\beta_{\ell(n-1)}}\right]\right\}$$
$$=\frac{h_{n-1}}{h_n}\left\{\bar{T}_{n+1}(s)\left[1+2\sum_{\ell=1}^{\infty}(-1)^{\ell}\frac{s}{s+\beta_{\ell n}}\right]-\bar{T}_n(s)\left[1+2\sum_{\ell=1}^{\infty}\frac{s}{s+\beta_{\ell n}}\right]\right\},$$
$$n=1,2,...,N, \tag{17}$$

in which $\bar{T}_n(s)$ is the Laplace transform of $T_n(\tau)$, defined by

$$\bar{T}_n(s)=\int_0^{\infty}\exp(-s\tau)T_n(\tau)\,\mathrm{d}\tau. \tag{18}$$

It is noted that $\bar{T}_0(s)=-T_0/s$ and $\bar{T}_{N+1}(s)=-T_b/s$ since $T_0(\tau)=-T_0$ and $T_{N+1}(\tau)=-T_b$. Hence, Equation (17) may be rewritten in compact form as

$$\sum_{n=1}^{N}a_{mn}(s)\bar{T}_n(s)=b_m(s),\quad m=1,2,...,N, \tag{19}$$

where $\bar{T}_n(s)$ are normalized by T_0, $a_{mn}(s)$ has a banded structure with the non-zero elements given by

$$a_{n(n-1)}(s)=-\frac{k_{n-1}}{k_n}G_{n-1}(s),\quad n=2,3,...,N,$$
$$a_{nn}(s)=\frac{k_{n-1}}{k_n}F_{n-1}(s)+\frac{h_{n-1}}{h_n}F_n(s),\quad n=1,2,...,N,$$
$$a_{n(n+1)}(s)=-\frac{h_{n-1}}{h_n}G_n(s),\quad n=1,2,...,N-1, \tag{20}$$

and the components of $b_m(s)$ are

$$b_1(s)=-\frac{k_0}{k_1}\frac{G_0(s)}{s},$$
$$b_N(s)=-\left(\frac{T_b}{T_0}\right)\frac{h_{N-1}}{h_N}\frac{G_N(s)}{s},$$
$$b_m(s)=0,\quad m=2,3,...,N-1, \tag{21}$$

where $F_n(s)$ and $G_n(s)$ are

$$F_n(s)=1+2s\sum_{\ell=1}^{\infty}\frac{1}{s+\beta_{\ell n}}=\frac{\sqrt{s}}{\gamma_n}\coth\frac{\sqrt{s}}{\gamma_n},\quad n=0,1,2,...,N, \tag{22}$$

$$G_n(s)=1+2s\sum_{\ell=1}^{\infty}\frac{(-1)^{\ell}}{s+\beta_{\ell n}}=\frac{\sqrt{s}}{\gamma_n}\frac{1}{\sinh\dfrac{\sqrt{s}}{\gamma_n}},\quad n=0,1,2,...,N, \tag{23}$$

respectively, in which the constants γ_n are defined by

$$\gamma_n = \sqrt{\frac{\kappa_n}{\kappa_0}}\left(\frac{b}{h_n}\right) = \sqrt{\frac{\beta_{\ell n}}{\ell^2\pi^2}}. \tag{24}$$

After $\bar{T}_n(s)$ are solved from (19), we may use inverse Laplace transform to get $T_n(\tau)$ in the time domain. In general, numerical inversion has to be invoked, however, there are difficulties with the numerical inverse Laplace transform. This is particularly true if all $\bar{T}_n(s)$ (n = 1, 2, ..., N) are simultaneously inverted since the numerical algorithms are generally not stable (Bellman et al., 1966). For instance, a small perturbation in $\bar{T}_n(s)$ may induce a large change in $T_n(\tau)$.

2.3. Asymptotic solution of temperature for short time

It is well known in the Laplace transform theory that one can obtain an approximate solution of the temperature for small values of time τ by inverting its Laplace transform for large values of s. Thus the asymptotic solutions of the interface temperatures $T_n(\tau)$ for small values of time τ are investigated next.

For large values of s, it is first noted that

$$\begin{aligned} &F_n(s) \to \frac{\sqrt{s}}{\gamma_n}, \quad s \to \infty, \\ &G_n(s) \to 2\frac{\sqrt{s}}{\gamma_n}\exp\left(-\frac{\sqrt{s}}{\gamma_n}\right), \quad s \to \infty. \end{aligned} \tag{25}$$

Substitution of the above expressions into (20) and (21) yields the first order expressions of $a_{n(n-1)}(s)$, $a_{nn}(s)$, $a_{n(n+1)}(s)$ and $b_1(s)$, $b_N(s)$ for large s as follows

$$\begin{aligned} &a_{n(n-1)}(s) \to a^0_{n(n-1)}\sqrt{s}\exp\left(-\frac{\sqrt{s}}{\gamma_{n-1}}\right), \quad s \to \infty, \\ &a_{nn}(s) \to a^0_{nn}\sqrt{s}, \quad s \to \infty, \\ &a_{n(n+1)}(s) \to a^0_{n(n+1)}\sqrt{s}\exp\left(-\frac{\sqrt{s}}{\gamma_n}\right), \quad s \to \infty, \end{aligned} \tag{26}$$

and

$$\begin{aligned} &b_1(s) \to \frac{b^0_1}{\sqrt{s}}\exp\left(-\frac{\sqrt{s}}{\gamma_0}\right), \quad s \to \infty, \\ &b_N(s) \to \left(\frac{T_b}{T_0}\right)\frac{b^0_N}{\sqrt{s}}\exp\left(-\frac{\sqrt{s}}{\gamma_N}\right), \quad s \to \infty, \end{aligned} \tag{27}$$

where the constants $a^0_{n(n-1)}$, a^0_{nn}, $a^0_{n(n+1)}$ and b^0_1, b^0_N are

$$\begin{aligned} &a^0_{n(n-1)} = -2\frac{k_{n-1}}{k_n}\frac{1}{\gamma_{n-1}}, \quad n = 2, 3, ..., N, \\ &a^0_{nn} = \frac{k_{n-1}}{k_n}\frac{1}{\gamma_{n-1}} + \frac{h_{n-1}}{h_n}\frac{1}{\gamma_n}, \quad n = 1, 2, ..., N, \\ &a^0_{n(n+1)} = -2\frac{h_{n-1}}{h_n}\frac{1}{\gamma_n}, \quad n = 1, 2, ..., N-1, \end{aligned} \tag{28}$$

and

$$b_1^0 = -2\frac{k_0}{k_1}\frac{1}{\gamma_0}, \quad b_N^0 = -2\frac{h_{N-1}}{h_N}\frac{1}{\gamma_N}. \tag{29}$$

With the above asymptotic expressions, the approximate solutions of $\bar{T}_n(s)$ for large values of s are obtained as follows

$$\begin{aligned}
&\bar{T}_n(s) = \bar{T}_n^{(1)}(s) + \left(\frac{T_b}{T_0}\right)\bar{T}_n^{(2)}(s), \quad n = 1, 2, ..., N,\\
&\bar{T}_n^{(1)}(s) = \frac{L_n^{(0)}}{s}\exp\left(-\sqrt{s}\sum_{i=1}^{n}\frac{1}{\gamma_{i-1}}\right),\\
&\bar{T}_n^{(2)}(s) = \frac{P_n^{(0)}}{s}\exp\left(-\sqrt{s}\sum_{i=n}^{N}\frac{1}{\gamma_i}\right), \quad n = 1, 2, ..., N,
\end{aligned} \tag{30}$$

where the constants $L_n^{(0)}$ and $P_n^{(0)}$ are

$$L_n^{(0)} = \tilde{b}_n^0/a_{nn}^0, \quad n = 1, 2, ..., N, \tag{31}$$

$$\begin{aligned}
&P_n^{(0)} = -\frac{a_{n(n+1)}^0}{a_{nn}^0}P_{n+1}^{(0)}, \quad n = 1, 2, ..., N-1,\\
&P_N^{(0)} = b_N^0/a_{NN}^0,
\end{aligned} \tag{32}$$

in which $\tilde{b}_n^0$ are given by

$$\begin{aligned}
&\tilde{b}_1^0 = b_1^0,\\
&\tilde{b}_n^0 = -\frac{a_{n(n-1)}^0}{a_{(n-1)(n-1)}^0}\tilde{b}_{n-1}^{(0)}, \quad n = 2, 3, ..., N.
\end{aligned} \tag{33}$$

By applying inverse Laplace transform to (30), we obtain the normalized interface temperatures $T_n(\tau)$ (normalized by T_0) for short time τ as follows

$$\begin{aligned}
&T_n(\tau) = T_n^{(1)}(\tau) + \left(\frac{T_b}{T_0}\right)T_n^{(2)}(\tau), \quad n = 1, 2, ..., N,\\
&T_n^{(1)}(\tau) = L_n^{(0)}\mathrm{erfc}\left(\frac{1}{2\sqrt{\tau}}\sum_{i=1}^{n}\frac{1}{\gamma_{i-1}}\right),\\
&T_n^{(2)}(\tau) = P_n^{(0)}\mathrm{erfc}\left(\frac{1}{2\sqrt{\tau}}\sum_{i=n}^{N}\frac{1}{\gamma_i}\right), \quad n = 1, 2, ..., N,
\end{aligned} \tag{34}$$

where $\mathrm{erfc}(\cdot)$ is the complementary error function defined by

$$\mathrm{erfc}(x) = 1 - \mathrm{erf}(x) = 1 - \frac{2}{\sqrt{\pi}}\int_0^x \exp(-y^2)\,\mathrm{d}y. \tag{35}$$

After obtaining the interface temperatures, the intra-layer temperatures (normalized by T_0) can be calculated by substituting (34) into (12). For the first layer (0th layer), the temperature

is given by

$$\begin{aligned} T(x^*,\tau) &= -(1-x^*)+x^*T_1(\tau)+ \\ &\quad +2\sum_{\ell=1}^{\infty}\frac{\sin(\ell\pi x^*)}{\ell\pi}\exp(-\beta_{\ell 0}\,\tau)+ \\ &\quad +2\sum_{\ell=1}^{\infty}(-1)^{\ell}\,\frac{\sin(\ell\pi x^*)}{\ell\pi}\left[I_{\ell 1}^{(3)}(\tau)+\left(\frac{T_b}{T_0}\right)I_{\ell 1}^{(4)}(\tau)\right]. \end{aligned} \tag{36}$$

For the last layer (Nth layer), the temperature is obtained by

$$\begin{aligned} T(x^*,\tau) &= (1-x^*)T_N(\tau)-x^*\left(\frac{T_b}{T_0}\right)- \\ &\quad -2\left(\frac{T_b}{T_0}\right)\sum_{\ell=1}^{\infty}(-1)^{\ell}\,\frac{\sin(\ell\pi x^*)}{\ell\pi}\exp(-\beta_{\ell N}\,\tau)- \\ &\quad -2\sum_{\ell=1}^{\infty}\frac{\sin(\ell\pi x^*)}{\ell\pi}\left[I_{\ell N}^{(1)}(\tau)+\left(\frac{T_b}{T_0}\right)I_{\ell N}^{(2)}(\tau)\right]. \end{aligned} \tag{37}$$

Finally, for the intermediate layers ($n = 1, 2, ..., N-1$), the temperature is

$$\begin{aligned} T(x^*,\tau) &= (1-x^*)T_n(\tau)+x^*T_{n+1}(\tau)- \\ &\quad -2\sum_{\ell=1}^{\infty}\frac{\sin(\ell\pi x^*)}{\ell\pi}\left[I_{\ell n}^{(1)}(\tau)+\left(\frac{T_b}{T_0}\right)I_{\ell n}^{(2)}(\tau)\right]+ \\ &\quad +2\sum_{\ell=1}^{\infty}(-1)^{\ell}\,\frac{\sin(\ell\pi x^*)}{\ell\pi}\left[I_{\ell(n+1)}^{(3)}(\tau)+\left(\frac{T_b}{T_0}\right)I_{\ell(n+1)}^{(4)}(\tau)\right]. \end{aligned} \tag{38}$$

The functions $I_{\ell n}^{(i)}$ ($i = 1, 2, 3, 4$; $n = 1, 2, ..., N$) in (36)–(38) are given by

$$I_{\ell n}^{(1)}(\tau)=\frac{L_n^{(0)}}{2\sqrt{\pi}}\left(\sum_{i=1}^{n}\frac{1}{\gamma_{i-1}}\right)\int_0^{\tau}(\tau')^{-\frac{3}{2}}\exp\left[-\beta_{\ell n}(\tau-\tau')-\frac{1}{4\tau'}\left(\sum_{i=1}^{n}\frac{1}{\gamma_{i-1}}\right)^2\right]\mathrm{d}\tau', \tag{39}$$

$$I_{\ell n}^{(2)}(\tau)=\frac{P_n^{(0)}}{2\sqrt{\pi}}\left(\sum_{i=n}^{N}\frac{1}{\gamma_i}\right)\int_0^{\tau}(\tau')^{-\frac{3}{2}}\exp\left[-\beta_{\ell n}(\tau-\tau')-\frac{1}{4\tau'}\left(\sum_{i=n}^{N}\frac{1}{\gamma_i}\right)^2\right]\mathrm{d}\tau', \tag{40}$$

$$I_{\ell n}^{(3)}(\tau)=\frac{L_n^{(0)}}{2\sqrt{\pi}}\left(\sum_{i=1}^{n}\frac{1}{\gamma_{i-1}}\right)\int_0^{\tau}(\tau')^{-\frac{3}{2}}\exp\left[-\beta_{\ell(n-1)}(\tau-\tau')-\frac{1}{4\tau'}\left(\sum_{i=1}^{n}\frac{1}{\gamma_{i-1}}\right)^2\right]\mathrm{d}\tau', \tag{41}$$

$$I_{\ell n}^{(4)}(\tau)=\frac{P_n^{(0)}}{2\sqrt{\pi}}\left(\sum_{i=n}^{N}\frac{1}{\gamma_i}\right)\int_0^{\tau}(\tau')^{-\frac{3}{2}}\exp\left[-\beta_{\ell(n-1)}(\tau-\tau')-\frac{1}{4\tau'}\left(\sum_{i=n}^{N}\frac{1}{\gamma_i}\right)^2\right]\mathrm{d}\tau'. \tag{42}$$

Equations (36)–(38) will be used to study thermal stresses and TSIFs in the FGM strip. Usually the series in these equations converge slowly. A linear interpolation may be used to

obtain the temperatures within the layers with satisfactory accuracy if a large number of layers is chosen. In this particular case, the series in (36)–(38) may be ignored, i.e., only the first line in each of these Equations (36)–(38) is considered to determine intra-layer temperatures.

3. Thermal stress

The temperature and mechanics analyses are uncoupled in this work, i.e. the temperature analysis is performed first, and the stress analysis is conducted afterwards. In the following study of thermal stresses in the FGM strip and TSIFs at the tip of an edge crack shown in Figure 1, a special kind of FGM is considered in which the Young's modulus and Poisson's ratio are constant. This assumption will limit the applications of the present analysis, however, there do exist some FGM systems, especially ceramic/ceramic FGMs, for which Young's modulus may be approximately assumed as constant. Examples include $MoSi_2/Al_2O_3$ system (Miyamoto et al., 1997) and TiC/SiC system (Sand et al., 1999). Ceramic/metal systems include zirconia/nickel FGM (Miyamoto, 1997; Moriya et al., 1999) whose Young's modulus may not change significantly because nickel alloys and partially stablized zirconia have similar Young's modulus, and zirconia/steel system (Kawasaki and Watanabe, 1993). The advantage of assuming a constant Young's modulus is that the crack analysis is simplified.

The FGM strip is assumed to undergo plane strain deformations and is free from constraints at the far away ends (see Figure 1). The only nonzero in-plane stress σ_{YY} is given by (Jin and Batra, 1996b)

$$\begin{aligned}\sigma_{YY}^{T}(X,\ \tau)\ =\ & -\frac{E\alpha(X)}{1-\nu}T(X,\ \tau)+\\ & +\frac{E}{(1-\nu^2)A_0}\left[(A_{22}-XA_{21})\int_0^b\frac{E\alpha(X')}{1-\nu}T(X',\ \tau)\,\mathrm{d}X'-\right.\\ & \left.-\ (A_{12}-XA_{11})\int_0^b\frac{E\alpha(X')}{1-\nu}T(X',\ \tau)X'\,\mathrm{d}X'\right],\end{aligned}\tag{43}$$

where E is Young's modulus, ν is Poisson's ratio, $\alpha(X)$ is the coefficient of thermal expansion, the superscript T in σ_{YY}^{T} stands for thermal stress, and $A_{ij}(i,\ j=1,2)$ and A_0 are given by

$$\begin{aligned}A_{11}&=\int_0^b\frac{E}{1-\nu^2}\,\mathrm{d}X=\frac{Eb}{1-\nu^2},\quad A_{12}=A_{21}=\int_0^b\frac{E}{1-\nu^2}X\,\mathrm{d}X=\frac{Eb^2}{2(1-\nu^2)},\\ A_{22}&=\int_0^b\frac{E}{1-\nu^2}X^2\,\mathrm{d}X=\frac{Eb^3}{3(1-\nu^2)},\quad A_0=A_{11}A_{22}-A_{12}A_{21}.\end{aligned}\tag{44}$$

By substituting the temperature solution (36)–(38) into (43), we obtain the normalized thermal stress in the strip

$$\begin{aligned}\frac{\sigma_{YY}^{T}(X,\ \tau)}{E\alpha_0T_0/(1-\nu)}&=-\frac{\alpha(X)}{\alpha_0}T(X,\ \tau)+\left(4-6\frac{X}{b}\right)\sum_{n=0}^{N}\left(\frac{h_n}{b}\right)\left(\frac{\alpha_n}{\alpha_0}\right)H_{n1}(\tau)-\\ &-\left(6-12\frac{X}{b}\right)\sum_{n=0}^{N}\left[\left(\frac{h_n}{b}\right)^2\left(\frac{\alpha_n}{\alpha_0}\right)H_{n2}(\tau)+\left(\frac{h_n}{b}\right)\left(\frac{X_n}{b}\right)\left(\frac{\alpha_n}{\alpha_0}\right)H_{n1}(\tau)\right],\end{aligned}\tag{45}$$

where α_n ($n = 0, 1, ..., N$) are the coefficients of thermal expansion in the nth layer and $H_{n1}(\tau)$ and $H_{n2}(\tau)$ are

$$H_{n1}(\tau) = \int_0^1 T(x^*,\ \tau)\,\mathrm{d}x^*, \quad H_{n2}(\tau) = \int_0^1 T(x^*,\ \tau)x^* dx^*. \tag{46}$$

in which $T(x^*,\ \tau)$ is the temperature in the nth layer given in (36)–(38).

4. Thermal stress intensity factor (TSIF)

Consider an edge crack in the FGM strip shown in Figure 1b. The boundary conditions for the thermal crack problem are

$$\sigma_{XX} = \sigma_{XY} = 0, \quad X = 0 \text{ and } X = b;\ Y \geq 0, \tag{47}$$

$$\sigma_{XY} = 0, \quad 0 \leq X \leq b,\ Y = 0, \tag{48}$$

$$v = 0, \quad a < X \leq b,\ Y = 0, \tag{49}$$

$$\sigma_{YY} = -\sigma_{YY}^T(X,\ \tau), \quad 0 \leq X \leq a,\ Y = 0, \tag{50}$$

where $\sigma_{YY}^T(X,\ \tau)$ is given in (45), v is the displacement in Y-direction, a and b are the crack length and the strip thickness, respectively. By using Fourier transform and integral equation methods, the above boundary value problem is reduced to the following singular integral equation

$$\int_{-1}^{1}\left[\frac{1}{s-r} + K(r,s)\right]\phi(s,\tau)\,\mathrm{d}s = -\frac{2\pi(1-\nu^2)}{E}\sigma_{YY}^T(X,\ \tau), \quad |r| \leq 1, \tag{51}$$

where the unknown density function $\phi(r, \tau)$ is

$$\phi(X,\tau) = \partial v(X,0,\tau)/\partial X, \tag{52}$$

with the notation $v \equiv v(X,\ Y,\ \tau)$, and $r = 2X/a - 1$, $s = 2X'/a - 1$. The kernel $K(r,\ s)$ is singular only at $(r,\ s) = (-1,\ -1)$ and is given by

$$K(X,\ X') = a\int_0^\infty f(X, X', \xi)\,\mathrm{d}\xi, \tag{53}$$

with $f(X, X', \xi)$ being given by

$$\begin{aligned}
f(X, X', \xi) \ = \ & -0.25/\left[1 - \left(2 + 4(b\xi)^2\right)\exp(-2b\xi) + \exp(-4b\xi)\right] \times \\
& \times \{[-1 - (1 - 2X'\xi)(3 - 2X\xi)]\exp[-(X + X')\xi] + \\
& + [(-(1 + 2X'\xi) + (3 + 2(b - X)\xi)(1 - 2b\xi(1 - 2(b - X')\xi)) + \\
& + (2 + 4(b\xi)^2)(1 - 2(b - X')\xi)]\exp[-(X - X' + 2b)\xi] + \\
& + [1 + (3 + 2(b - X)\xi)(1 + 2(b - X')\xi)]\exp[-(X + X' + 2b)\xi] + \\
& + [-4 - 2X'\xi + 2X\xi]\exp[-(X - X' + 4b)\xi] + \\
& + [1 + (1 - 2(b - X')\xi)(3 - 2(b - X)\xi)]\exp[-(2b - X - X')\xi] + \\
& + [(3 - 2(b - X)\xi)(-1 + 2b\xi(1 - 2X'\xi)) - (1 - 2X'\xi)] \times \\
& \times \exp[-(X' - X + 2b)\xi] + \\
& + [-(3 - 2(b - X)\xi)(1 + 2X'\xi) + (1 - 2b\xi(1 - 2(b - X')\xi)) - \\
& - (2 + 4(b\xi)^2)]\exp[-(4b - X - X')\xi] + \\
& + [4 - 2X'\xi + 2X\xi]\exp[-(X' - X + 4b)\xi]\}.
\end{aligned}$$

The function $\phi(r, \tau)$ can be further expressed as (Gupta and Erdogan, 1974)

$$\phi(r, \tau) = \psi(r, \tau)/\sqrt{1 - r}, \tag{54}$$

where $\psi(r, \tau)$ is continuous and bounded for $r \in [-1,\ 1]$. When $\phi(r, \tau)$ is normalized by $(1 + \nu)\alpha_0 T_0$, the normalized TSIF, K^*, at the crack-tip is obtained as

$$K^* = \frac{(1 - \nu)K_I}{E\alpha_0 T_0\sqrt{\pi b}} = -\frac{1}{2}\sqrt{\frac{a}{b}}\,\psi(1, \tau), \tag{55}$$

where K_I denotes the mode I TSIF.

5. FGM material properties

A two phase ceramic/metal or ceramic/ceramic FGM is considered here. Since the Young's modulus and Poisson's ratio are assumed constant, only thermal properties are of concern. Usually, the effective properties of an FGM are calculated from that of its constituent materials and the volume fractions by means of a micromechanical model. Though such model is not available for FGMs yet, some models for conventional homogeneous composite materials may be utilized with reasonable accuracy (Reiter et al., 1997; Reiter and Dvorak, 1998; Dvorak and Srinivas, 1999). The FGM is assumed as a two phase composite material with graded volume fractions of its constituent phases.

The thermal conductivity of the FGM, $k(X)$, is

$$k(X) = k_m\left[1 + \frac{V_i(X)(k_i - k_m)}{k_m + (k_i - k_m)(1 - V_i(X))/3}\right], \tag{56}$$

where the subscripts i and m stand for the inclusion and matrix properties, respectively, and $V_i(X)$ is the volume fraction of the inclusion phase. The effective property (56) was obtained by Hashin and Shtrikman (1962) for a composite spheres model, and by Christensen (1979) in the context of the three phase model, a generalized self-consistent scheme. In actual FGMs, there may be no distinct matrix and inclusion phases in a region, however, (56) is still used to approximate the thermal conductivity of the FGM.

The mass density of the FGM, $\rho(X)$, is described by a rule of mixtures

$$\rho(X) = V_i(X)\rho_i + (1 - V_i(X))\rho_m. \tag{57}$$

The coefficient of thermal expansion of the FGM, $\alpha(X)$, is also calculated from the rule of mixtures

$$\alpha(X) = V_i(X)\alpha_i + (1 - V_i(X))\alpha_m. \tag{58}$$

which is reduced from the general result of two-phase composites (Levin, 1968) for the special case that the two phases have identical elastic bulk moduli.

The specific heat of the FGM, $c(X)$, is assumed to follow the rule of mixtures in this work

$$c(X) = V_i(X)c_i + (1 - V_i(X))c_m. \tag{59}$$

With the thermal properties and mass density of the FGM given by (56)–(59), the temperatures, thermal stresses and TSIFs can be calculated from (36)–(38), (45) and (55) for various

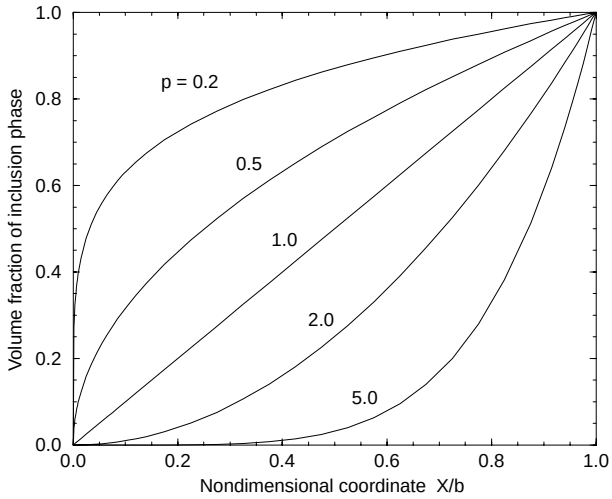

Figure 2. Volume fractions of the inclusion phase in an FGM strip.

Table 1. Material Properties of TiC and SiC.

Materials	Young's modulus (GPa)	Poisson's ratio	Coefficient of thermal expansion ($10^{-6}\ K^{-1}$)	Thermal conductivity ($W\ m^{-1}\ K^{-1}$)	Mass density ($g\ cm^{-3}$)	Specific heat ($J\ g^{-1}\ K^{-1}$)
TiC	400	0.2	7.0	20	4.9	0.7
SiC	400	0.2	4.0	60	3.2	1.0

volume fraction profiles $V_i(X)$. The volume fraction, $V_i(X)$, is assumed in the form of a power function, i.e.,

$$V_i(X) = (X/b)^p. \tag{60}$$

Thus $X = 0$ corresponds to pure matrix phase and $X = b$ is pure inclusion material. Figure 2 shows the volume fraction of the inclusion phase for various values of p.

6. Numerical results and discussion

In the following numerical calculations, a TiC/SiC FGM is considered. The material properties of the titanium carbide (TiC) and the silicon carbide (SiC) are listed in Table 1 (Munz and Fett, 1999; Sand et al., 1999). This is a ceramic/ceramic FGM with potential applications in areas such as cutting tools and turbines. In most cases, we will assume that the thermally shocked edge $X = 0$ is pure TiC (as the matrix phase) and the opposite edge is pure SiC. We also only consider the case of $T_b/T_0 = 0$, i.e. $T_b = 0$ and $T_0 \neq 0$. This represents a severe thermal shock load on the strip, which is important for engineering applications.

6.1. TEMPERATURE FIELD

The temperature in the FGM strip is calculated from the asymptotic solution (36)–(38). To obtain an idea to what extent the temperature can be approximated by (36)–(38), these equations are first applied to a homogeneous strip where each layer has identical material properties. The results are plotted against the following complete temperature solution (normalized by T_0) for a homogeneous strip (Carslaw and Jaeger, 1959),

$$T(X,\ \tau) = -1 - \left(\frac{T_b}{T_0} - 1\right)\frac{X}{b} - 2\sum_{\ell=1}^{\infty}\frac{(T_b/T_0)(-1)^{\ell} - 1}{\ell\pi}\sin\left(\frac{\ell\pi X}{b}\right)\exp(-\ell^2\pi^2\tau). \tag{61}$$

Since the series in (36)–(38) converge very slowly, a linear interpolation is used to calculate the intra-layer temperatures. Figure 3a shows the normalized temperatures at different nondimensional time τ for a 20 layer model where the layers have equal thickness. Figure 3b shows the results for a 30 layer model (equal thickness). It is seen from Figure 3 that the asymptotic solution and the complete solution are almost identical in the entire range of the strip for nondimensional times up to $\tau = 0.05$. Those solutions also agree well with each other in the entire strip for times up to $\tau = 0.10$. For times up to $\tau = 0.15$, the solutions are in good agreement in the region of $X/b < 0.6$. The results are almost the same for the 20 and 30 layers models which shows that convergent results are obtained. It will be seen in the following subsections that the thermal stress in the strip and the TSIF reach their maximum values before the normalized time of $\tau = 0.10$. Hence, the asymptotic solution (36)–(38) offers a reliable basis to obtain the maximum thermal stress and the maximum TSIF.

Figure 4 shows normalized temperatures in both the homogeneous strip and FGM strip for volume fraction profiles p = 0.2, 1.0 and 2.0 (see (60) and Figure 2). The layered model consists of 45 layers with more layers intensively deployed near the edge X = 0 as the compositional profile of the FGM varies dramatically near the edge $X = 0$ in the case of $p = 0.2$ (see Figure 2). *The 45 layer model is used in all calculations of temperatures, thermal stresses and TSIFs for the FGM strip.* Figure 4a depicts the temperatures at $\tau = 0.001$. It is seen that the temperature remains at the initial value ($T = 0$) in the region $0.2 < X/b \leq 1$. Moreover, the temperature drops to the boundary value of -1 rapidly near the thermally shocked edge $X = 0$. The temperature in the FGM strip for both $p = 1$ and $p = 2$ is almost identical to that in a homogeneous strip. Figure 4b shows the temperature profiles at $\tau = 0.01$, in which case the temperature starts dropping around the middle of the strip. Figure 4c gives the temperature at a longer time $\tau = 0.1$, and, in this case, the temperature decays within the full width of the strip.

6.2. THERMAL STRESS

The normalized thermal stresses in the FGM strip are calculated from the asymptotic solution (45). For verification purposes, Equation (45) is first applied to a homogeneous material. Figure 5 shows the normalized thermal stresses computed from (45) and the following solution

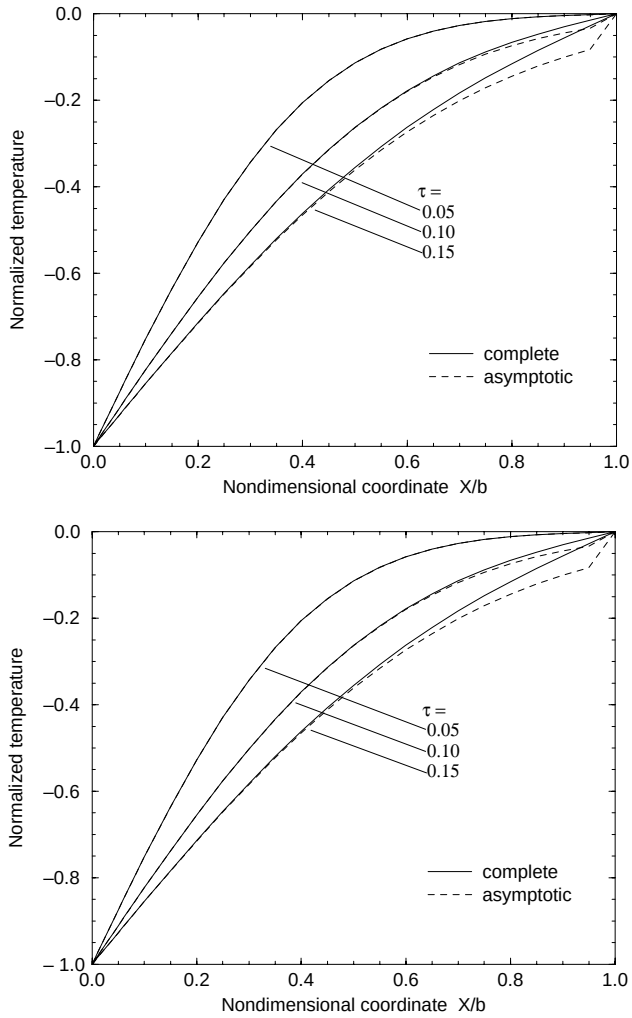

Figure 3. Temperature distribution in a homogeneous strip: asymptotic solution versus complete solution. (a) 20 layers; (b) 30 layers.

based on the 'complete' temperature field (61) for a homogeneous strip

$$\frac{\sigma_Y^T(X,\ \tau)}{E\alpha_m T_0/(1-\nu)} = 2\sum_{\ell=1}^{\infty}\frac{(T_b/T_0)(-1)^\ell - 1}{\ell\pi}\sin\left(\frac{\ell\pi X}{b}\right)\exp(-\ell^2\pi^2\tau) -$$
$$-2\left(4-6\frac{X}{b}\right)\sum_{\ell=1}^{\infty}\frac{(T_b/T_0)(-1)^\ell - 1}{\ell\pi}\frac{1-(-1)^\ell}{\ell\pi}\exp(-\ell^2\pi^2\tau) +$$
$$+2\left(6-12\frac{X}{b}\right)\sum_{\ell=1}^{\infty}\frac{(T_b/T_0)(-1)^\ell - 1}{\ell\pi}\frac{(-1)^{\ell+1}}{\ell\pi}\exp(-\ell^2\pi^2\tau). \quad (62)$$

It is seen that the asymptotic solution agrees well with the complete solution for times up to $\tau = 0.10$ in the entire strip. Figure 6 shows the normalized thermal stresses in both the homogeneous strip and the FGM strip for the volume fraction profiles p = 0.2, 1.0 and 2.0 (see (60) and Figure 2). Figure 6a depicts the thermal stresses at $\tau = 0.001$, and Figures 6b

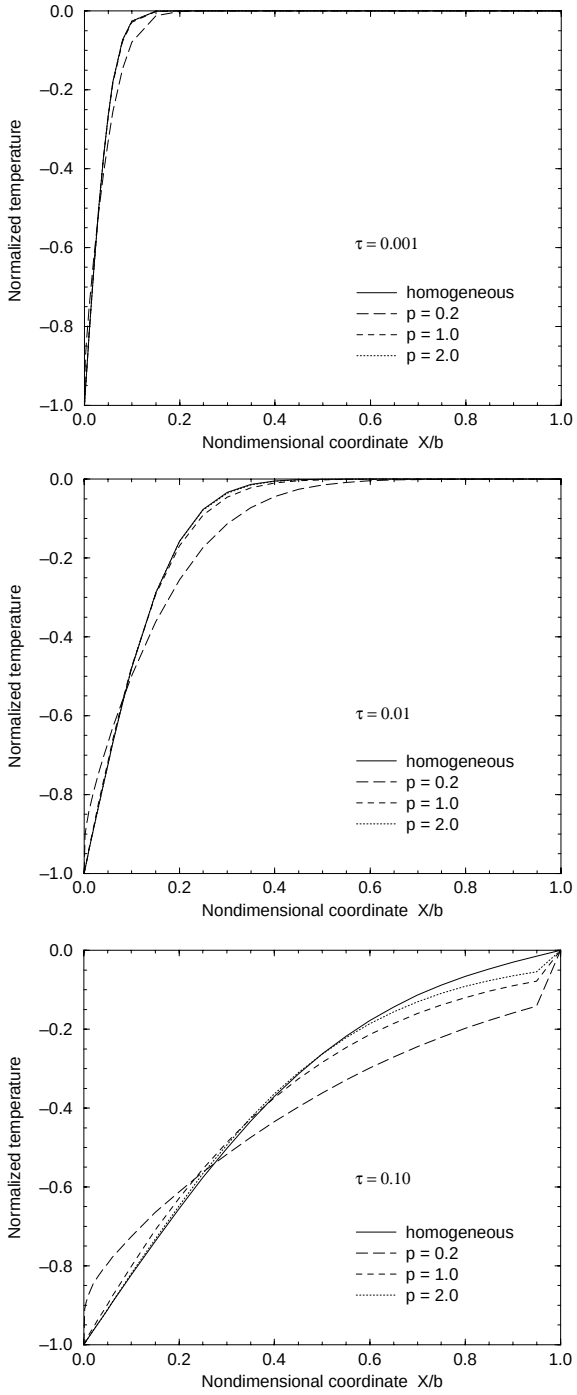

Figure 4. Temperature distribution in the FGM strip for various times. (a) τ = 0.001; (b) τ = 0.01; (c) τ = 0.10.

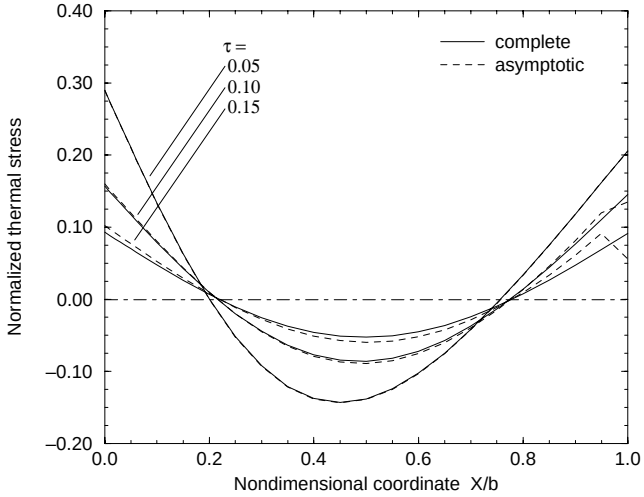

Figure 5. Thermal stresses in a homogeneous strip: asymptotic solution versus complete solution.

and 6c show the results at times $\tau = 0.01$ and $\tau = 0.1$, respectively. As in the homogeneous case, tensile stresses develop in the edge regions of the FGM strip and compressive stresses develop in the middle portion. It is observed that at each time, the thermal stress reaches the peak value at $X = 0$. The thermal stress in the FGM strip for $p = 0.2$ decreases from its peak value sharply near the thermally shocked edge $X = 0$ with an increase in X. It is noted that the peak thermal stress in the homogeneous strip decreases with increasing time faster than that in the FGM strip (cf., Figures 6a to 6c). Therefore, the thermal stress near $X = 0$ in the FGM strip may be higher than that in the homogeneous strip for a delayed time (see Figure 6c). However, the peak thermal stress in the FGM strip is almost identical to that in the homogeneous strip for very small τ. For example, the normalized peak thermal stresses (at $X = 0$) in the FGM strip for $p = 0.2$ are 0.9587, 0.8778, 0.6763 and 0.4484 for times τ = 0.0001, 0.001, 0.01 and 0.1, respectively. The corresponding peak values in the homogeneous strip are 0.9549, 0.8632, 0.6087 and 0.1569, respectively. The stress plot for the shortest time $\tau = 0.0001$ is not provided here.

6.3. THERMAL STRESS INTENSITY FACTOR (TSIF)

As in the case of thermal stresses, the TSIF of an edge crack in a homogeneous strip is first studied based on both the asymptotic temperature (36)–(38) and the complete solution (61). The normalized TSIF calculated based on the complete temperature field has the following characteristics: for a given normalized crack length a/b, the TSIF increases with time, reaches a peak value at a particular time which increases with the crack length (i.e., the time to reach the peak TSIF for a longer crack is larger than that for a shorter crack), and then decreases with further increase of time. There exists a critical crack length $l_c = a_c/b$ at which the peak TSIF reaches a maximum. The TSIF based on the asymptotic temperature solution also has these characteristics.

Figure 7a shows the normalized TSIFs for edge cracks with lengths of a/b = 0.1, 0.3 and 0.5 in a homogeneous strip based on both (36)–(38) and the complete temperature field (61). It is seen that the TSIFs based on the asymptotic solution are in good agreement with that based on the complete solution for times up to approximate $\tau = 0.1$, and it is clear that the

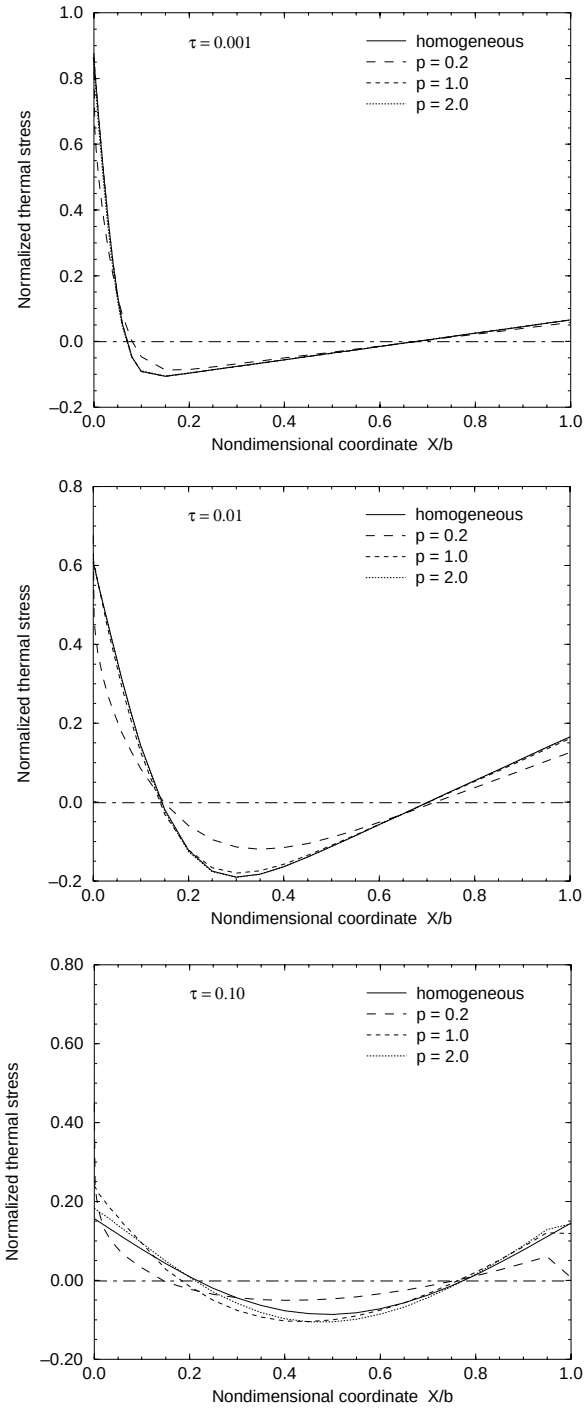

Figure 6. Thermal stresses in the FGM strip for various times. (a) τ = 0.001; (b) τ = 0.01; (c) τ = 0.10.

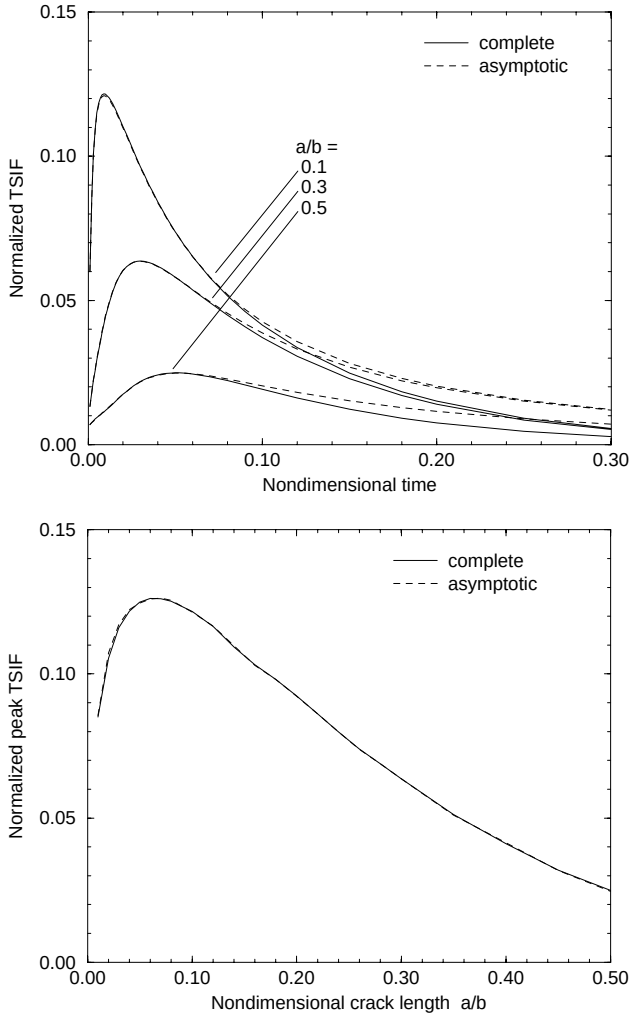

Figure 7. (a), Thermal stress intensity factor for a homogeneous strip: asymptotic solution versus complete solution; (b), Peak thermal stress intensity factor for a homogeneous strip: asymptotic solution versus complete solution.

peak TSIFs occur at times less than $\tau = 0.1$. *Thus the asymptotic solution is able to capture the peak TSIF.* Figure 7b shows the peak TSIFs for cracks of lengths up to $a/b = 0.5$ in the homogeneous strip. It is evident that the peak TSIFs based on the asymptotic temperature solution agree very well with those based on the complete temperature solution. The next paragraph discusses both the limitations and range of applications of the present approach.

It is noted that the TSIF may reach its peak at times greater than $\tau = 0.1$ for long cracks if a finite heat transfer coefficient on the surface of the strip is adopted (see, for example, the discussion of Lu and Fleck (1998) for a homogeneous solid). In addition, when a 'hot' thermal shock (i.e., the surface of the FGM strip is subjected to heating instead of cooling) is considered, the thermal stress in the central region of the FGM strip will be positive and the TSIF for a short interior crack may reach the peak at times greater than $\tau = 0.1$. The present asymptotic solution for short times is mostly useful for FGM strips with large heat transfer cofficients when subjected to 'cold' thermal shocks and with short edge cracks. The thermal

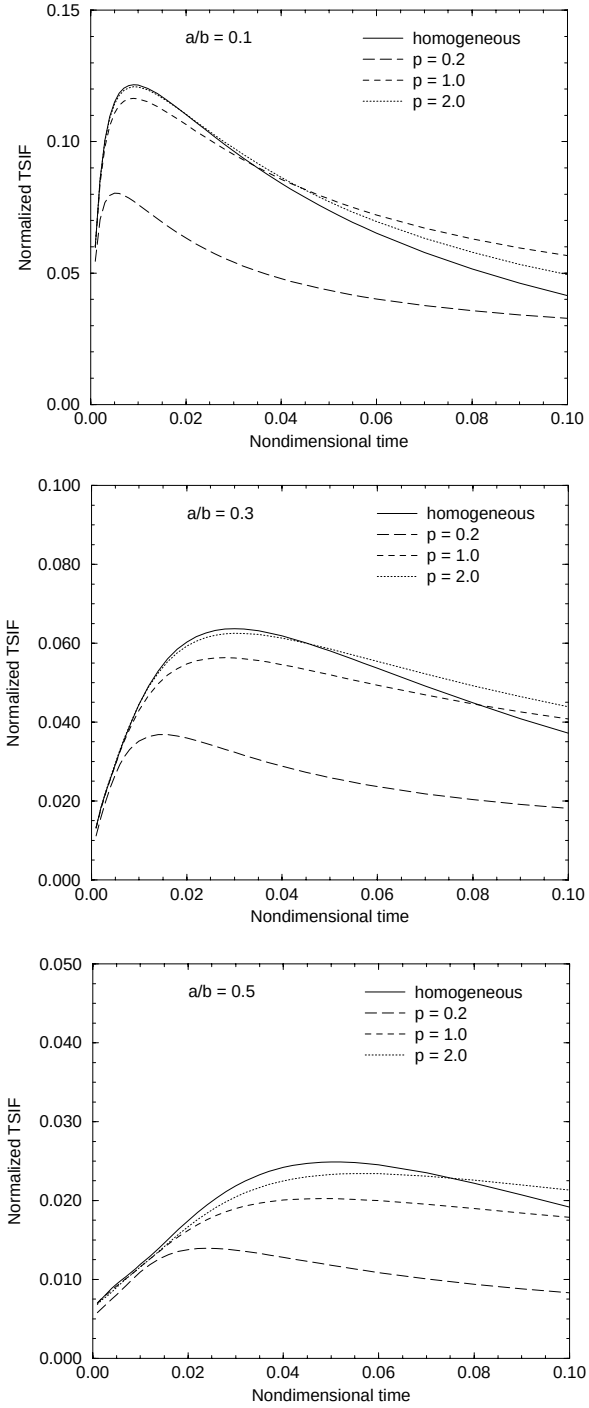

Figure 8. Thermal stress intensity factor for the FGM strip for various crack lengths. (a) $a/b = 0.1$; (b) $a/b = 0.3$; (c) $a/b = 0.5$.

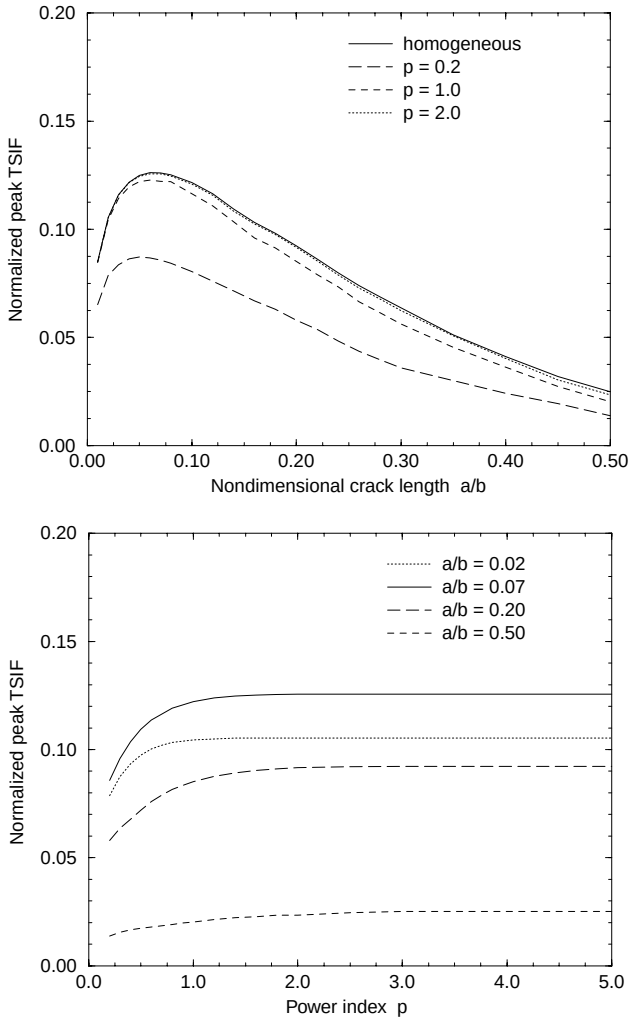

Figure 9. (a) Peak thermal stress intensity factor versus crack length for the FGM strip; (b) Peak thermal stress intensity factor versus power index p of the inclusion volume fraction for the FGM strip.

stress in an FGM strip subjected to a 'cold' shock with infinite heat transfer cofficient is the most severe and, in general, a short edge crack is most dangerous because the TSIF at the crack tip is significantly larger than those of interior cracks.

Figure 8 shows the normalized TSIF versus nondimensional time τ for cracks in both the homogeneous strip and the FGM strip for the volume fraction profiles p = 0.2, 1.0 and 2.0 (see (60) and Figure 2). Figure 8a shows the results for a/b = 0.1, and Figures 8b and 8c show the results for a/b = 0.3 and 0.5, respectively. Some relevant observations can be made from these figures. First, the TSIF for cracks in the FGM strip varies with time and crack length in a similar way to that of the TSIF for a homogeneous strip, i.e., for a given normalized crack length a/b, the TSIF increases with time, reaches a peak value at a particular time that increases with the crack length, and then decreases with further increase of time (see introductory paragraph of this Section). There exists a critical crack length $l_c^{\mathrm{FGM}} = a_c^{\mathrm{FGM}}/b$ at which the peak TSIF reaches a maximum. The time at which the FGM TSIF reaches the peak decreases with decreasing power index p of the volume fraction of SiC. Second, the TSIF for

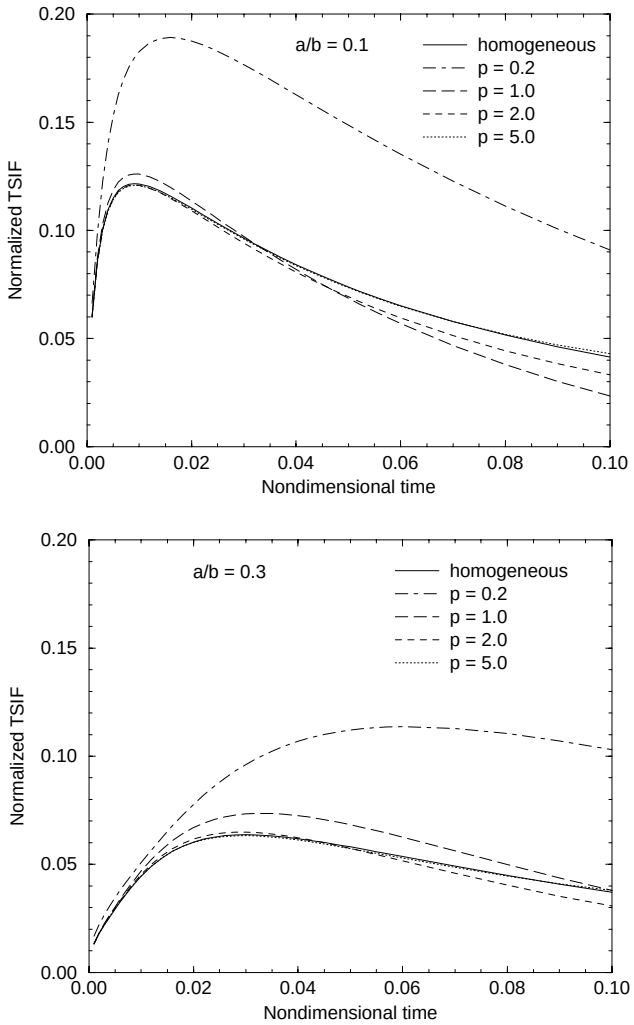

Figure 10. Thermal stress intensity factor for the FGM strip with SiC as the matrix phase. (a) $a/b = 0.1$; (b) $a/b = 0.3$.

the FGM is lower than that for the homogeneous strip for short times, but may be higher than that for the homogeneous strip for extended times. Moreover, the peak TSIF for the FGM is lower than that for the homogeneous strip.

Figure 9a shows the normalized peak TSIFs for both the homogeneous and the FGM strips. It is observed that the maximum of the peak TSIFs occurs at about $a/b = 0.07$ for the homogeneous strip and at slightly short crack lengths for the FGM. Figure 9b shows the effect of p on the peak TSIF for the FGM strip. It is seen that the peak TSIF changes little for $p \geq 2$ but decreases with decreasing p for smaller p. The maximum normalized TSIF for the FGM strip with $p = 0.2$ is about 0.08713 while the corresponding value for the homogeneous strip is about 0.1261.

For all above calculations, we have assumed that the thermally shocked edge of the strip ($X = 0$) is pure TiC and the opposite edge ($X = b$) is pure SiC. Now we consider the TSIF for the reverse situation where $X = 0$ is pure SiC and $X = b$ is pure TiC. Figures 10a

and 10b show the normalized TSIF for edge cracks in this FGM for the cases $a/b = 0.1$ and $a/b = 0.3$, respectively. It is observed that, in general, the TSIF for the FGM strip is actually higher than that for the homogeneous strip and increases with decreasing p which now represents the power index of TiC volume fraction. The results may be due to the fact that the thermal conductivity of TiC is lower than that of SiC. Thus care must be exercised in designing such FGM system so that the thermally shocked edge is TiC.

7. Conclusions

A multi-layered material model is employed to solve the temperature field in a strip of a functionally graded material subjected to transient thermal loading conditions. The FGM is assumed having constant Young's modulus and Poisson's ratio, but the thermal properties of the material vary along the thickness direction of the strip. This kind of FGMs include some ceramic/ceramic FGMs such as TiC/SiC, $MoSi_2/Al_2O_3$ and $MoSi_2$/SiC, and also some ceramic/metal FGMs such as zirconia/nickel and zirconia/steel. By using Laplace transform and an asymptotic analysis, an analytical first order temperature solution for short times is obtained. For a homogeneous strip, the asymptotic solution for temperature agrees well with the complete solution for nondimensional times up to about $\tau = 0.10$, and so do the thermal stress and the TSIF of an edge crack. It is noted that the peak TSIF occurs at times less than $\tau = 0.1$. The thermal stresses and the TSIFs of edge cracks are calculated for a TiC/SiC FGM with various volume fraction profiles of SiC represented by the power index p. It is found that the peak TSIF decreases with a decrease in p if the thermally shocked cracked edge of the FGM strip is pure TiC, whereas the TSIF is increased if the thermally shocked edge is pure SiC.

Acknowledgements

We would like to acknowledge the support from the National Science Foundation (NSF) under grant No. CMS-9996378 (Mechanics & Materials Program).

References

Aboudi, J., Pindera, M.J. and Arnold, S.M. (1997). Microstructural optimization of functionally graded composites subjected to a thermal gradient via the coupled higher-order theory. *Composites Part B – Engineering* **28**, 93–108.

Bao, G. and Wang, L. (1995). Multiple cracking in functionally graded ceramic/metal coatings. *International Journal of Solids and Structures* **32**, 2853–2871.

Bellman, R., Kalaba, R.E. and Lockett, J.A. (1966). *Numerical Inversion of Laplace Transform.* American Elsevier Publishing Company, INC., New York.

Cai, H. and Bao, G. (1998). Crack bridging in functionally graded coatings. *International Journal of Solids and Structures* **35**, 701–717.

Carpenter, R.D., Liang, W.W., Paulino, G.H., Gibeling, J.C. and Munir, Z.A. (1999). Fracture testing and analysis of a layered functionally graded Ti/TiB beam in 3-point bending. *Materials Science Forum* **308–311** (edited by W.A. Kaysser), Trans Tech Publications, Switzerland, 837–842.

Carslaw, H.S. and Jaeger, J.C. (1959). *Conduction of Heat in Solids*, Clarendon Press, Oxford.

Choi, H.J., Jin, T.E. and Lee, K.Y. (1998). Collinear cracks in a layered half-plane with a graded nonhomogeneous interfacial zone – Part II: Thermal shock response. *International Journal of Fracture* **94**, 123–135.

Christensen, R.M. (1979). *Mechanics of Composite Materials.* John Wiley & Sons, New York.

Delale, F. and Erdogan, F. (1983). The crack problem for a nonhomogeneous plane. *ASME Journal of Applied Mechanics* **50**, 609–614.

Drake, J.T., Williamson, R.L. and Rabin, B.H. (1993). Finite element analysis of thermal residual stresses at graded ceramic-metal interfaces, Part II: interface optimization for residual stress reduction. *Journal of Applied Physics* **74**, 1321–1326.

Dvorak, G.J. and Srinivas, M.V. (1999). New estimates of overall properties of heterogeneous solids. *Journal of the Mechanics and Physics of Solids* **47**, 899–920.

Erdogan, F. (1995). Fracture mechanics of functionally graded materials. *Composites Engineering* **5**, 753–770.

Erdogan, F. and Wu, B.H. (1996). Crack problems in FGM layers under thermal stresses. *Journal of Thermal Stresses* **19**, 237–265.

Erdogan, F. and Wu, B.H. (1997). The surface crack problem for a plate with functionally graded properties. *ASME Journal of Applied Mechanics* **64**, 449–456.

Georgiadis, H.G., Barber, J.R. and Benammar, F. (1991). An asymptotic solution for short-time transient heat-conduction between 2 dissimilar bodies in contact. *Quarterly Journal of Mechanics and Applied Mathematics* **44**, 303–322.

Giannakopoulos, A.E., Suresh, S., Finot, M. and Olsson, M. (1995). Elastoplastic analysis of thermal cycling: layered materials with compositional gradient. *Acta Metallurgica Materialia* **43**, 1335–1354.

Gray, L.J. and Paulino, G.H. (1997). Symmetric Galerkin boundary integral formulation for interface and multi-zone problems. *International Journal for Numerical Methods in Engineering* **40**, 3085–3101.

Gu, P. and Asaro, R.J. (1997a). Cracks in functionally graded materials. *International Journal of Solids and Structures* **34**, 1–17.

Gu, P. and Asaro, R.J. (1997b). Crack deflection in functionally graded materials. *International Journal of Solids and Structures* **34**, 3085–3098.

Gupta, G.D. and Erdogan, F. (1974). The problem of edge cracks in an infinite strip. *ASME Journal of Applied Mechanics* **41**, 1001–1006.

Hashin, Z. and Shtrikman, S. (1962). A variational approach to the theory of the effective magnetic permeability of multiphase materials. *Journal of Applied Physics* **33**, 3125.

Hasselman, D.P.H. and Youngblood, G.E. (1978). Enhanced thermal stress resistance of structural ceramics with thermal conductivity gradient. *Journal of the American Ceramic Society* **61**, 49–52.

Hirai, T. (1996). Functionally gradient materials. *Materials Science and Technology*, **17B:** *Processing of Ceramics, Part 2* (edited by R.J. Brook), VCH Verlagsgesellschaft mbH, Weinheim, Germany, 292–341.

Honein, T. and Herrmann, G. (1997). Conservation laws in nonhomogeneous plane elastostatics. *Journal of the Mechanics and Physics of Solids* **45**, 789–805.

Jin, Z.-H. and Batra, R.C. (1996a). Some basic fracture mechanics concepts in functionally graded materials. *Journal of the Mechanics and Physics of Solids* **44**, 1221–1235.

Jin, Z.-H. and Batra, R.C. (1996b). Stress intensity relaxation at the tip of an edge crack in a functionally graded material subjected to a thermal shock. *Journal of Thermal Stresses* **19**, 317–339.

Jin, Z.-H. and Batra, R.C. (1998). *R*-curve and strength behavior of a functionally graded material. *Materials Science and Engineering* **A242**, 70–76.

Jin, Z.-H. and Noda, N. (1994a). Crack tip singular fields in nonhomogeneous materials. *ASME Journal of Applied Mechanics* **61**, 738–740.

Jin, Z.-H. and Noda, N. (1994b). Transient thermal stress intensity factors for a crack in a semi-infinite plane of a functionally gradient material. *International Journal of Solids and Structures* **31**, 203–218.

Joachim-Ajao, D. and Barber, J. R. (1998). Effect of material properties in certain thermoelastic contact problems. *ASME Journal of Applied Mechanics* **65**, 889–893.

Kawasaki, A. and Watanabe, R. (1987). Finite element analysis of thermal stress of the metals/ceramics multi-layer composites with controlled compositional gradients. *Journal of Japan Institute of Metals* **51**, 525–529.

Kawasaki, A. and Watanabe, R. (1993). Fabrication of disk-shaped functionally gradient materials by hot pressing and their thermomechanical performance. *Ceramic Transactions, Vol. 34, Functionally Gradient Materials* (edited by J.B. Holt, M. Koisumi, T. Hirai and Z.A. Munir), American Ceramic Society, Westerville, Ohio, 157–164.

Koizumi, M. (1993). The concept of FGM. *Ceramic Transactions, Vol. 34, Functionally Gradient Materials* (edited by J.B. Holt, M. Koisumi, T. Hirai and Z.A. Munir), American Ceramic Society, Westerville, Ohio, 3–10.

Kokini, K. and Case, M. (1997). Initiation of surface and interface edge cracks in functionally graded ceramic thermal barrier coatings. *ASME Journal of Engineering Materials and Technology* **119**, 148–152.

Kokini, K. and Choules, B.D. (1995). Surface thermal fracture of functionally graded ceramic coatings: effect of architecture and materials. *Composites Engineering* **5**, 865–877.

Kuroda, Y., Kusaka, K., Moro, A. and Togawa, M. (1993). Evaluation tests of ZrO_2/Ni functionally gradient materials for regeneratively cooled thrust engine applications. *Ceramic Transactions, Vol. 34, Functionally Gradient Materials* (edited by J.B. Holt, M. Koisumi, T. Hirai and Z.A. Munir), American Ceramic Society, Westerville, Ohio, 289–296.

Levin, V.M. (1968). On the coefficients of thermal expansion of heterogeneous material. *Mekh. Tverd. Tela* **88** (in Russian).

Lu, T.J. and Fleck, N.A. (1998). The thermal shock resistance of solids. *Acta Materialia* **46**, 4755–4768.

Miyamoto, Y. (1997). Application of FGMs in Japan. *Ceramic Transactions,* **76:** *Functionally Graded Materials* (edited by A. Ghosh, Y. Miyamoto, I. Reimanis and J.J. Lannutti), American Ceramic Society, Westerville, Ohio, 171–189.

Miyamoto, Y., Kang, Y., Tanihara, K., Lin, J., Niino, M., Hirai, S. and Umakoshi, T. (1997). Application of Graded $MoSi_2/Al_2O_3/Ni/Al_2O_3/ MoSi_2$ to high temperature electrode of SiGe thermoelectric device. *Ceramic Transactions, Vol. 76, Functionally Graded Materials* (edited by A. Ghosh, Y. Miyamoto, I. Reimanis and J.J. Lannutti), American Ceramic Society, Westerville, Ohio, 135–148.

Moriya, S., Kuroda, Y., Sato, M., Tadano, M., Moro, A. and Niino, M. (1999). Research on the application of PSZ/Ni FGM thermal barrier coating to the combustion chamber (damage conditions of TBC and its mechanism). *Materials Science Forum* **308–311**, (edited by W.A. Kaysser), Trans Tech Publications, Switzerland, 410–415.

Munz, D. and Fett, T. (1999). *Ceramics*, Springer-Verlag, Berlin.

Noda, N. (1997). Thermal stress intensity factor for functionally gradient plate with an edge crack. *Journal of Thermal Stresses* **20**, 373–387.

Noda, N. and Jin, Z.-H. (1993). Thermal stress intensity factors for a crack in a strip of a functionally gradient material. *International Journal of Solids and Structures* **30**, 1039–1056.

Ozisik, M.N. (1980). *Heat Conduction*, John Wiley & Sons, New York.

Paulino, G.H., Fannjiang, A.C. and Chan, Y.S. (1999). Gradient elasticity theory for a Mode III crack in a functionally graded material. *Materials Science Forum* **308–311**, (edited by W.A. Kaysser), Trans Tech Publications, Switzerland, 971–976.

Reddy, J.N. and Chin, C.D. (1998). Thermomechanical analysis of functionally graded cylinders and plates. *Journal of Thermal Stresses* **21**, 593–626.

Reiter, T. and Dvorak, G.J. (1998). Micromechanical models for graded composite materials: II. thermomechanical loading. *Journal of the Mechanics and Physics of Solids* **46**, 1655–1673.

Reiter, T., Dvorak, G.J. and Tvergaard, V. (1997). Micromechanical models for graded composite materials. *Journal of the Mechanics and Physics of Solids* **45**, 1281–1302.

Sand, Ch., Adler J. and Lenk, R. (1999). A new concept for manufacturing sintered materials with a three dimensional composition gradient using a silicon carbide - titanium carbide composite. *Materials Science Forum* **308–311**, (edited by W.A. Kaysser), Trans Tech Publications, Switzerland, 65–70.

Schovanec, L. and Walton, J.R. (1988). On the order of stress singularity for an antiplane shear crack at the interface of two bonded inhomogeneous elastic materials. *ASME Journal of Applied Mechanics* **55**, 234–236.

Suresh, S. and Mortensen, A. (1998). *Fundamentals of Functionally Graded Materials.* The Institute of Materials, London.

Takahashi, H., Ishikawa, T., Okugawa, D. and Hashida, T. (1993). Laser and plasma-ARC thermal shock/fatigue fracture evaluation procedure for functionally gradient materials. *Thermal Shock and Thermal Fatigue Behavior of Advanced Ceramics* (edited by G.A. Schneider and G. Petzow), Kluwer Academic Publishers, Dordrecht, 543–554.

Tanigawa, Y., Akai, T., Kawamura, R. and Oka, N. (1996). Transient heat conduction and thermal stress problems of a nonhomogeneous plate with temperature-dependent material prperties. *Journal of Thermal Stresses* **19**, 77–102.

Tanihara, K., Miyanoto, Y., Matsushita, K., Ma, X., Kawasaki, A., Watanabe, R. and Hirano, K. (1993). Fabrication of Cr_3C_2/Ni functionally gradient materials by gas-pressure combustion sintering. *Ceramic Transactions, Vol. 34, Functionally Gradient Materials* (edited by J.B. Holt, M. Koisumi, T. Hirai and Z.A. Munir), American Ceramic Society, Westerville, Ohio, 361–369.